The *Pseudomonas aeruginosa* Wsp pathway undergoes positive evolutionary selection during chronic infection

Erin S. Gloag[1¶], Christopher W. Marshall[2, 3¶], Daniel Snyder[2, 3], Gina R. Lewin[4, 5], Jacob S. Harris, Sarah B. Chaney[1], Marvin Whiteley[4, 5], Vaughn S. Cooper[2, 3], Daniel J. Wozniak[1,6] *

[1] Department of Microbial Infection and Immunity, The Ohio State University, Columbus, OH, USA

[2] Department of Microbiology and Molecular Genetics, University of Pittsburgh School of Medicine, Pittsburgh, PA, USA

[3] Center for Evolutionary Biology and Medicine, University of Pittsburgh School of Medicine, Pittsburgh, PA, USA

[4] School of Biological Sciences, Georgia Institute of Technology, Atlanta, GA, USA

[5] Emory-Children's Cystic Fibrosis Center, Atlanta, GA, USA

[6] Department of Microbiology, The Ohio State University, Columbus, OH, USA

* Corresponding author: Daniel J. Wozniak

Email: Daniel.Wozniak@osumc.edu

[¶] These authors contributed equally to this work

Running title: Evolution of *P. aeruginosa* RSCVs in a chronic infection model

Author Contributions: ESG and CWM performed the experimental work. JSH performed the colony PCR. SBC infected and sampled the porcine burn wounds. DS generated the sequence library. MW and GRL quantified the strain frequency in the wounds. ESG, CWM, MW, VSC, and DJW conceptualized the project and wrote the manuscript.

Introductory paragraph (200 words)

Pathogens experience pressure in an infection to adapt, with selection favoring mutants that persist. *Pseudomonas aeruginosa* commonly adapts by evolving mutants with hyper-biofilm production that evade clearance. Despite our understanding of the adaptive phenotypes, studying their emergence and dynamics in an infection has proven challenging. Here we used a porcine full-thickness burn wound model of chronic infection to study how mixed strains of *P. aeruginosa* adaptively evolve. Wounds were infected with six *P. aeruginosa* strains, including the model PA14 strain (PA14-1), and biopsies taken at 3, 14, and 28 days post-infection. Rugose small-colony variants (RSCVs) were detected at 3-d and persisted, with the majority evolved from PA14-1. Whole genome sequencing of PA14-1 RSCVs revealed driver mutations exclusively in the *wsp* pathway. RSCVs also acquired CRISPR-Cas adaptive immunity to prophages isolated from the *P. aeruginosa* wound isolate (B23-2) present in the inoculum. The rapid rise of RSCVs to detectable frequencies is evidence of positive selection of the Wsp chemosensory system and suggests that RSCVs may arise earlier in an infection than originally appreciated, to facilitate infection. Given the prevalence of RSCVs in chronic infections, we predict that RSCVs may be a common, early adaptation during infections.

Chronic infections are those that persist despite extensive treatment. These persistent infections are often attributed to difficult to eradicate biofilms, which are communities of adhered microorganisms encased in an extracellular polymeric substance (EPS) [1,2]. Complicating chronic infections is the high likelihood that bacterial populations adaptively evolve, producing persistent phenotypes with increased fitness.

One of the most understood bacterial adaptive responses to chronic infection is that of *Pseudomonas aeruginosa* to the cystic fibrosis (CF) lung [3]. CF patients exhibit mucus accumulation, where *P. aeruginosa* biofilms commonly colonize the mucus lining and establish persistent pulmonary infections [4-6]. Evolved phenotypic variants of this organism are routinely isolated from CF patient sputum samples, and several of these variants are often associated with worsening patient prognosis [7]. Of particular interest are the rugose small-colony variants (RSCVs), which are isolated from up to 50% of *P. aeruginosa*-positive CF sputum samples [8,9]. When isolated, their frequencies range drastically between 0.1 − 100% [9,10]. In contrast there is little-to-no reports of the frequency of *P. aeruginosa* adapted variants from other chronic infections, such as chronic wound infections.

Common to RSCVs are mutations in pathways that lead to elevated cyclic diguanylate monophosphate (c-di-GMP) [7]. C-di-GMP is a messenger molecule that signals the transition from planktonic to biofilm lifestyle in many bacteria [11]. In *P. aeruginosa*, increased c-di-GMP, among many responses, leads to overproduction of exopolysaccharides, Psl and Pel, and matrix proteins [12,13]. As a result, RSCVs have hyper-biofilm phenotypes [13,14], increased tolerance to antimicrobials [10], and enhanced resistance to immunity [15,16]. *P. aeruginosa* RSCVs also evolve from *in vitro* grown biofilms [17,18], suggesting that there is strong selection for ecological diversification in both *in vivo* and *in vitro* biofilms.

RSCVs with driver mutations in the Wsp pathway, particularly *wspF,* are commonly isolated from CF sputum and *in vitro* biofilms [12,19]. The Wsp (wrinkly spreader) pathway is a chemosensory system that regulates c-di-GMP in response to surface sensing. Upon detecting a surface, the methyl-accepting chemotaxis protein (MCP), WspA, is methylated by the methyltransferase, WspC. WspA then interacts with the histidine kinase, WspE, which phosphorylates the diguanylate cyclase (DGC) WspR, resulting in c-di-GMP synthesis [20-23]. The methylesterase, WspF, de-methylates WspA, re-setting the system. Therefore, in *wspF* loss of function mutants, WspA remains methylated and the Wsp pathway continually activated, leading to overproduction of c-di-GMP [24].

Despite our understanding of the divergent phenotypes of evolved variants, studying their emergence and the selective pressures driving their evolution *in vivo* is challenging, as there are few chronic infection models that mimic what is observed clinically. To address this challenge, we used a porcine full-thickness thermal injury wound model, which closely reflects human clinical chronic wounds [25,26]. Furthermore, chronic infection models typically only address the adaptive traits of a single founding clone, but susceptible individuals are constantly exposed to different strains of opportunistic pathogens. Here we used the porcine wound model in a *P. aeruginosa* mixed strain infection to understand which strains become prevalent and how they undergo genetic and phenotypic diversification.

Results

P. aeruginosa strains PA14-1 and PAO1-B11 become dominant in a *P. aeruginosa* mixed-strain chronic burn wound infection

To determine relative fitness of different *P. aeruginosa* strains and if the population evolves in a chronic infection, we infected porcine full-thickness burn wounds with an

111 inoculum consisting of approximately equal numbers of 6 different *P. aeruginosa*
112 strains. Wounds were infected with 2 model strains (PA14-1 and PAO1-B11), 3
113 clinical isolates (B23-2, CF18-1 and S54485-1), and a water isolate (MSH10-2) (Fig
114 1A, Table S1). Each strain had a unique nucleotide barcode introduced at the neutral
115 *Tn7* site (Table S1). These strains share similar metabolic kinetics (Fig S1A, B) and
116 biofilm formation capacity (Fig S1C). Biopsies were taken 3-, 14-, and 28-d post-
117 infection for bacterial quantification (Fig S2).
118
119 Colony forming units (CFU) revealed a high bacterial burden at both 3-d and 14-d
120 post infection. However, the bacterial levels from 14-d biopsies were more variable
121 across replicates (Fig 1B), suggesting wounds had begun clearing the infection.
122 Wounds remained colonized at approximately 10^5 bacteria up to 28-d (Fig 1B). To
123 quantify the proportion of each strain across the sampled timepoints, genomic DNA
124 was isolated from biopsy tissue and sequenced. As early as 3-d post infection, PA14-
125 1 and PAO1-B11 were the predominant strains in the infection, outcompeting the 4
126 other strains present (Fig 1C).
127
128 **_P. aeruginosa_ evolves RSCVs during porcine chronic burn wound infections**
129 To determine if adapted *P. aeruginosa* variants emerged, we used colony
130 morphologies as an indicator. Homogenized biopsies were grown on Vogel-Bonner
131 minimal media supplemented with Congo red and brilliant blue (VBMM). RSCVs,
132 defined by a matte, rugose colony morphology that stained intensely by the two dyes,
133 indicating exopolysaccharide overproduction, were isolated from all three timepoints
134 (Fig 2A). Two RSCV sub-populations were observed; one that had a pink, rugose
135 phenotype and a second that had an orange, textured phenotype (Fig 2A).
136
137 The RSCV abundance in the wounds was quantified by expressing their frequency
138 as a percentage of the total *P. aeruginosa* burden. The RSCV frequency was low in

the wounds on 3-d (0.02 ± 0.12%) before peaking at 14-d, with a frequency of approximately 2% (2.15 ± 5.25%) (Fig 2B). On 28-d, the RSCV frequency decreased to 0.19 ± 0.65% of the total bacterial burden (Fig 1B, 2B). To determine if RSCVs experienced selective pressure in the wound, we calculated the selection coefficient, relative to the inoculum, at each timepoint across a range of possible starting frequencies according to equation (1). RSCVs showed significant positive selection across all time points with s >0.1 (Fig 2C). Selection of RSCVs was similar across all possible ranges on 3-d, while on 14-d and 28-d there was a gradual increase in selection coefficients. Despite the RSCV frequency decreasing on 28-d (Fig 2B), the RSCVs still showed significant positive selection in order to rise from undetectable frequencies to nearly 0.2% at 28-d (Fig 2C). This indicates that across all time points, RSCVs are adaptive.

RSCVs only evolved from the model strains PA14-1 and PAO1-B11 (Fig 2D). These also corresponded to the two RSCV phenotypes that were observed, with the pink RSCVs evolving from PA14-1, and the orange from PAO1-B11 (Fig 2A). RSCVs derived from PA14-1 were isolated across all timepoints and PAO1-B11 evolved RSCVs isolated from 14-d and 28-d. At the later two timepoints, PA14-1 RSCVs remained the predominant sub-population (Fig 2D).

Whole genome sequencing reveals that PA14-1 RSCVs contain driver mutations exclusively within the *wsp* pathway

As PA14-1 RSCVs were the predominate evolved phenotype, we focused on this sub-population for the remainder of the study. A description of the PAO1-B11 variants will be communicated elsewhere. Whole genome sequencing was performed on 27 randomly selected PA14-1 RSCVs to identify the mutation(s) accounting for the RSCV phenotype.

166

167 We identified putative driver mutations exclusively in the *wsp* cluster, specifically,
168 small deletions in *wspA* and *wspF.* (Table 1). We identified an in-frame 42bp deletion
169 (Δ285 − 298aa) in *wspA* (*wspA* Δ285-298), and a frame-shift 5bp deletion (Δ461 −
170 465bp) in *wspF* (*wspF* V154fs) (Table 1). RSCVs with the *wspA* mutation were
171 predominant across all timepoints, with *wspF* mutants only identified on 14-d. Using
172 RSCV-2 as a representative *wspA* mutant, the variant *wspA* was replaced on the
173 genome by a wildtype copy. This resulted in the RSCV colony phenotype reverting to
174 wildtype (Fig 3), demonstrating that the *wspA* Δ285-298 mutation is responsible for
175 the RSCV phenotype.

176

177 Some of the RSCVs also possessed secondary mutations (Table 1), demonstrating
178 further evolution in the wound. Two *wspA* RSCVs from 3-d (Table 1; RSCV-1 and
179 RSCV-4) acquired a 14,299bp deletion that removed the remaining *psl* operon. PA14
180 naturally lacks Psl, since *pslA* – *pslD* are absent [27]. In these two isolates the
181 remaining genes of the *psl* operon, *pslE* – *pslO* were deleted. Both of these PA14-1
182 RSCVs were isolated from the same wound, however from separate biopsied tissue,
183 suggesting that each deletion may have been a separate event. In the RSCV-1
184 background, complementation of *wspA* reverted the RSCV colony phenotype to
185 wildtype (Fig 3), indicating that deletion of the remaining *psl* operon did not influence
186 the RSCV phenotype.

187

188 Evidence of further evolution of the *wsp* cluster was detected on 28-d. RSCV-40, in
189 addition to having the *wspA* Δ285-298 driver mutation, had 3 separate mutations in
190 *wspD* which led to an early stop codon. This unusual mutation cluster is consistent
191 with error-prone translesion synthesis or DNA template switching facilitated by micro-

192 homology [28]. However, as the mutations occur at the *wspD* 3' end, the WspD N-
193 terminus may still be expressed and functional (Fig S3). WspD is a chaperone, which
194 along with WspB, are predicted to tether WspA and WspE [21]. In this isolate,
195 complementation of *wspA* reverted the RSCV colony phenotype to wildtype (Fig 3),
196 indicating that the *wspD* mutations did not influence the RSCV phenotype. However,
197 this further points towards the strong selective pressure on the Wsp pathway in the
198 chronic infection.

199

200 As the driver mutations occurred in the *wsp* pathway, we predicted that the RSCV
201 phenotype was due to overproduction of c-di-GMP. Using both a c-di-GMP *gfp*
202 reporter [29] and a plasmid encoding the phosphodiesterase PA2133, we determined
203 that both *wspA* and *wspF* mutants had elevated c-di-GMP levels compared to the
204 ancestor PA14-1, and that elevated c-di-GMP levels was responsible for the RSCV
205 colony phenotypes (Supplementary Results; Fig S4). These mutants also showed
206 increased biofilm formation and outcompeted the ancestor strain when grown in *in*
207 *vitro* planktonic and biofilm competition assays, with greater fitness values seen in
208 the biofilm (Supplementary Results; Fig S5). The presence of secondary mutations
209 did not appear to influence these phenotypes *in vitro*.

210

211 We were also interested in identifying how the PA14-1 non-RSCV population
212 adapted to the infection, and if this population acquired mutations that did not result
213 in divergent colony phenotypes. When we sequenced randomly selected PA14-1
214 non-RSCV isolates, relatively few had acquired chromosomal mutations
215 (Supplemental Results; Table S2). These isolates had similar levels of biofilm
216 formation and metabolic kinetics compared to the ancestor strain (Supplemental
217 Results; Fig S7), suggesting that the RSCVs were the major evolved sub-population
218 within the wounds.

WspA Δ285-298 mutation leads to auto-induction of the Wsp pathway

As the *wspA* Δ285-298 was the most common driver mutation, we investigated how it may lead to elevated c-di-GMP production. We observed that flanking the junctions of this deletion was a direct repeat at 837-854bp and 921-938bp (Fig S8; bold text [12]).

The WspA Δ285-298 mutation occurs between the predicted HAMP domain (histidine kinases, adenylate cyclases, methyl accepting proteins, and phosphatases) and the signaling domain (SD; Fig 4A). MCP cytoplasmic domains are comprised of consecutive 7aa heptads [30]. MCPs are defined into classes based on the number of heptads in the cytoplasmic domain [30], with *P. aeruginosa* WspA belonging to the 40H (40 heptads) MCP class [31]. The 285-298aa (14aa) deletion results in complete deletion of heptads N19 and N16 (Fig 4B).

To observe the localization of the deletion in the protein structure and gain insight into how the Δ285-298 mutation may alter the function and signaling of WspA, we generated a homology model of PA14 WspA against the *Thermotoga maritima* MCP (PDB 3JA6; [32]) (Fig 4C). Our homology model is also supported by the WspA Phyre secondary structure prediction [33] (Fig S9). Based on the model, the region of the deletion is predicted to occur opposite the methylation site (Fig 4C). We predict that the deletion could de-stabilize or alter the methylation site resulting in auto-induction of WspA and sustained WspR activation.

Evidence of inter-pseudomonad competition mediated by phages in chronic infections

Two PA14-1 RSCVs, RSCV-12 and RSCV-38, acquired a 60bp insertion at the clustered regularly interspaced short palindromic repeat (CRISPR) – CRISPR-associated proteins (Cas) locus (Table 1). Both sequences inserted at the intergenic region (-1549/+271) between PA14_33350 (RS13600) and PA14_33370 (RS13605) at the genomic position 2,937,205. The last 28bp of inserted sequence was identical between the two isolates and aligned to the repetitive elements in the PA14 CRISPR array (CRISPR2 [34]) (Fig 5A). However, the first 32bp differed, indicative of CRISPR spacer sequences (Fig 5A), which are specific to infective mobile genetic elements [35]. A BLAST search of the inserted CRISPR spacer against the ancestor strains identified that both insertions aligned to different contigs from strain B23-2 (See Supplemental Results; Fig S10).

We therefore predicted that RSCV-12 and -38 would be resistant to phages isolated from B23-2 due to CRISPR-Cas-acquired adaptive immunity. To test this, we grew B23-2 in mitomycin C and harvested the phage-enriched supernatant. *P. aeruginosa* strains were incubated with the phage lysate and plaque assays were performed. RSCV-12 and RSCV-38 displayed resistance to phage infection. RSCV-38 showed resistance across all replicates (Fig 5B). For RSCV-12, a single plaque was observed in 1 replicate, however for the remaining 3 replicates no plaques were observed (Fig 5B). This indicates that the acquired CRISPR spacers in RSCV-12 and RSCV-38 produced immunity to phages isolated from B23-2. Infection of RSCV-6 and RSCV-36 ($CRISPR^-$), which have the same driver mutation as RSCV-12 and RSCV-38 ($CRISPR^+$) respectively, revealed that RSCVs were not natively more resistant to phage infection compared to the ancestor strain (Fig 5B). The ancestor strain susceptibility was also determined to assess the host range of the isolated phages. As expected, B23-2 was resistant to phage infection, while the remaining strains

showed varying levels of phage sensitivity (CF18-1>MSH10-2, S54485-1>PA14-1, PAO1-B11; Fig 5C).

Discussion

Here we describe the rapid evolution of adaptive *P. aeruginosa* mutants with conspicuous colony phenotypes arising in a clinically relevant model of chronic infection. There is a consensus in the field that variants arise in an infection as a consequence of adaptation over extended periods of time. However, we isolated RSCVs from early stages of infection, suggesting that variants may evolve more rapidly than originally appreciated. This suggests that RSCVs may be a common, early adaptation during infections and that the selective pressures driving RSCV evolution may persist across these infections.

Even though wounds were infected with six different *P. aeruginosa* strains, we only isolated RSCVs evolved from PA14-1 and PAO1-B11 (Fig 2C). We predict this is due to PA14-1 and PAO1-B11 outcompeting the remaining four strains early in the infection (Fig 1C). *P. aeruginosa* RSCVs were selected in the infection and in *in vitro* conditions (Fig 2C, S5B). The selection coefficients determined here were up to 5 times greater than those identified in the Lenski long-term evolution lines [36], pointing towards the strong positive selection experienced by RSCVs. Furthermore, *Burkholderia cenocepacia* variants containing *wsp* mutations isolated from an *in vitro* biofilm evolution assay similarly showed high selection coefficients [37]. This suggests that *wsp* mutants experience significant positive selection both *in vivo* and *in vitro* environments. Despite these strong selection coefficients, RSCVs remained at relatively low frequencies in the infection (Fig 2B). This suggests that RSCVs show negative frequency dependence, that is, they exert a strong advantage at low frequencies, but are disadvantageous at high frequencies. Negative frequency dependent selection has been previously observed for evolved rugose variants of *P.*

299 *fluorescens* [38-40]. Niche competition [38,39] and division of labor [40] with the ancestor
300 strain drove the evolution of *P. fluorescens* rugose variants from static planktonic and
301 colony growth respectively. In both cases, diversification of the population was
302 maintained by negative frequency dependent selection [38-40]. The low frequency
303 RSCVs would likely facilitate the ancestor strain in colonizing and establishing
304 biofilms in the wound. We predict that in heterogeneous fitness landscapes, such as
305 those encountered during infection, there are niche environments where the low
306 frequency RSCVs would experience positive dependent frequency selection and
307 become more common. In support of this hypothesis is the observation that the
308 higher RSCV frequencies observed in CF patients are correlated to prolonged
309 exposure to antimicrobials, particularly aerosolized antibiotics [8,41].
310
311 All the sequenced PA14-1 RSCVs had driver mutations in the *wsp* cluster. This
312 indicates that in chronic wounds the Wsp pathway specifically undergoes selection,
313 and that *wsp* mutants may be more fit than other c-di-GMP-regulating pathways that
314 confer the RSCV phenotype. The *wspA* Δ285-298 was the most common driver
315 mutation and was isolated early in the infection (Table 1). There are two potential
316 explanations for the rapid rise of this single *wspA* mutant in the infection. The first is
317 that it may have been present in the initial inoculum at undetectable levels. The
318 second is that this region may be hyper-mutable owing to the direct repeat (Fig S8).
319 We are currently unable to discern between these two scenarios; however, it is
320 significant that the population rapidly diversifies in the wound due to strong positive
321 selection of adaptive phenotypes provided by *wsp* mutations.
322
323 Supporting the second theory is the observation that this region in *wspA* also
324 appears to be under selection in driving RSCV evolution during *in vitro* grown biofilms
325 (Fig S11). The *P. aeruginosa* PAO1 RSCV isolate MJK8, which evolved during
326 biofilm growth in a tube reactor [13], has an in-frame 66bp deletion (Δ286 – 307aa) in

the same region as *wspA* Δ285-298 [12]. *P. fluorescens* Pfl01 when grown as a colony biofilm evolved RSCVs with driver mutations identified in *wspC*, *wspA* and *wspE* [40]. One of the *wspA* mutations was a in-frame 84bp deletion (Δ284 – 311aa) again occurring in the homologous region [40]. Finally, *B. cenocepacia* HI2424 RSCVs with *wspA* and *wspE* mutations were isolated from a biofilm bead evolution experiment [37]. While the majority of mutations identified were non-synonymous SNPs, one of the *wspA* mutations was an in-frame 21bp deletion (Δ307-313aa) again in the homologous region [37] (Fig S11). We predict that these four deletions alter how WspA is methylated/demethylated and ultimately lead to constitutive signaling and auto-induction of the Wsp pathway.

In addition to driver mutations, some PA14-1 RSCVs also gained secondary mutations. Of particular interest was the Δ14,299bp, which deleted the remaining *psl* operon (Table 1; RSCV-1). We predicted that this deletion might lead to increased fitness of the RSCVs over the RSCV driver mutation alone. However, deletion of the remaining *psl* operon did not provide additional fitness benefits under the simple conditions tested. This suggests that in PA14 the remaining *psl* operon (*pslE* – *pslO*) may play a role outside of Psl synthesis, which may have a fitness cost in the wound environment.

Additional secondary mutations of interest were the 60bp insertions in the CRISPR-Cas array of RSCV-12 and RSCV-38 (Table 1, Fig 5A), which encoded resistance to phage(s) isolated from B23-2 (Fig 5C). It has only recently been confirmed that the *P. aeruginosa* type I-F CRISPR-Cas system provides adaptive immunity to phages with a target protospacer [42]. This is dependent on the presence of the correct protospacer adjacent motif (PAM) in the mobile genetic element [42]. In support of this, both protospacers contain the type I-F CRSIPR-Cas specific GG PAM (Fig S10).

354 Furthermore, B23-2 contig-107 contained two additional protospacers to which
355 CRISPR spacers in *P. aeruginosa* have been reported (Table S3, Fig S10A). Of
356 interest was the observation that PA14 already contains a CRISPR spacer identical
357 to a protospacer in contig-107 (Table S3, Fig S10A). This suggests that PA14 had
358 already been exposed to the prophage in B23-2. However, the ancestral PA14-1 was
359 still sensitive to infection (Fig 5B, C), presumably due to the incorrect PAM (Fig
360 S10A). This highlights the importance of insertion of the correct CRISPR spacer in
361 mediating phage immunity. This is only the second report of CRISPR-Cas acquired
362 immunity in *P. aeruginosa* strains [42] and to our knowledge the first report of CRISPR-
363 Cas adaptive immunity acquired in an infection.
364
365 Our data indicate that *P. aeruginosa* experiences strong selective forces in chronic
366 infections, and in response rapidly evolve during the initial stages of infection. RSCVs
367 containing mutations in the *wsp* cluster were the main adapted sub-population
368 isolated from all wounds. This indicates that the Wsp system is the main pathway
369 under selection to evolve adapted variants. This is despite other pathways in c-di-
370 GMP regulation being implicated in RSCV formation, both *in vivo* and *in vitro* [43-47].
371 We predict that RSCVs may be an adaptation common to chronic infections and
372 developing therapies that target the RSCV sub-population or prevent their
373 emergence could be transferrable across these infections.
374
375 **Materials and Methods**
376 **Bacterial strains, plasmids and media**
377 Bacterial strains and plasmids used in this study are detailed in Table S1. Gene
378 mutant constructs were made using Gibson Assembly (NEB) [48]. Primers used to
379 create the constructs are detailed in Table S4. These were incorporated into the *P.*
380 *aeruginosa* genome using two-step allelic recombination as previously described [49].
381

382 *P. aeruginosa* strains were maintained on LANS (Luria agar no salt; 10g/L tryptone,
383 5g/L yeast extract solidified with 1.5% agar) unless otherwise specified. RSCV colony
384 morphology was observed on adjusted Vogel-Bonner minimal media (0.2g/L
385 $MgSO_4 \bullet 7H_2O$, 3.5g/L $NaNH_4HPO_4 \bullet 4H_2O$, 10g/L K_2HPO_4, 0.1g/L $CaCl_2$, 2g/L citric
386 acid, 1g/L casamino acid, 40µg/mL Congo red, 15µg/mL brilliant blue, solidified with
387 1% agar; VBMM).
388
389 For *E. coli* strains, 10µg/mL gentamicin (gent), 100µg/mL ampicillin (amp) or
390 15µg/mL tetracycline (tet) was used for selection where appropriate. For *P.*
391 *aeruginosa* strains, 100µg/mL gent, 300µg/mL carbenicillin (carb) or 100µg/mL tet
392 was used for selection where appropriate.
393
394 **Porcine full-thickness chronic burn wound model**
395 Swine were housed and studied according to the protocols approved by the
396 Institutional Animal Care and Use Committee (IACUC) at The Ohio State University.
397
398 Porcine full-thickness chronic burn wound model was performed as previously
399 described [25]. Briefly, 2 pigs were subjected to thermal injury to achieve 6 full-
400 thickness (third-degree) burns bilaterally and covered with impermeable wound
401 dressings. Burn wounds were infected 3 days post injury with equal amounts of 6
402 different *P. aeruginosa* strains to achieve a final 250µL inoculum at 10^8 bacteria (1.6
403 $x10^7$ each for a total of 1×10^8). The 250µL inoculum was spread over the wounds
404 and allowed to air dry before the wound dressing was re-applied. Wounds were
405 infected with PA14-1, PAO1-B11, B23-2, CF18-1 (GenBank ID; NZ_KI519281),
406 MSH10-2 (GenBank ID; NZ_KE138672) and S54485-1 (GenBank ID; NZ_KI519256).
407 Prior to infection, each strain had been tagged with a unique barcode at the Tn7 site
408 on the genome (see Supplementary Materials and Methods; Table 1).
409

Wound healing was monitored 3, 14, and 28 days post infection. At each timepoint, 4-8 8mm punch biopsies were taken from 2 wounds on each pig (4 wounds for each timepoint, Fig S2). Biopsies were homogenized in 1mL PBS and plated on *Pseudomonas* isolation agar (PIA) supplemented with 100µg/mL gent for CFUs/ g tissue. To screen for the emergence of adapted *P. aeruginosa* variants, homogenized tissue was also plated onto VBMM supplemented with 100µg/mL gent. Colony morphology variants were passaged onto PIA followed by two rounds on non-selective LANS, before being plated back onto VBMM (without antibiotics) to confirm that the variant phenotype was a result of a stable mutation. Confirmed colony variants were stored at −80°C.

The selection of RSCVs in the wound was determined by calculating the selection coefficient (*s*) according to equation (1) [50]

$$s = \frac{\ln\left(\frac{N_{mx}}{N_{m0}}\right) - \ln\left(\frac{N_{wtx}}{N_{wt0}}\right)}{T_x} \qquad (1)$$

where T_x is day x, N is the number of cells, m is the mutant and wt is the wildtype at day x and day 0.

Colony morphology

1µL of overnight culture was spotted on VBMM plates and incubated at 37°C for 24h. Colonies were imaged on a Stereo Microscope (AmScope) fitted with a Microscope Digital Color CMOS camera (AmScope). Images were processed in FIJI [51].

Sequencing and analysis

To determine the frequency of each strain across the infection, genomic DNA was isolated from porcine tissue and the barcodes were sequenced as follows. Tissue was added to 2mL Goodman's buffer A (100 mM NaCl, 100 mM Tris-HCl pH 8, 10

435 mM EDTA pH 8, 3.33% SDS, 0.1% sodium deoxycholate) in a bead beater tube with
436 0.1mm glass beads and 2-3mm zirconia beads. The tissue was lysed by placing
437 tubes in a TissueLyser II (QIAGEN) for 30s at 50Hz. This was repeated 4 times,
438 placing tubes on ice for 30s in between each lysis round to prevent tubes from
439 overheating. Lysed tissue was incubated with 50µL proteinase K (20mg/mL) for 3h at
440 55°C. 2mL of phenol, chloroform, isomyl alcohol solution (25:24:1, pH 8) was added
441 and samples were centrifuged for 5min at room temperature. The aqueous phase
442 was removed and mixed with 1.5mL isopropanol. Sample was incubated for 30min at
443 -20°C before being centrifuged for 30min at 4°C. The pellet was washed in 1mL 75%
444 EtOH and again centrifuged. EtOH was removed and the DNA pellet air-dried and
445 resuspended in 500µL sterile water. Strain-specific barcodes were amplified and
446 given Illumina sequencing adapters using Tn7_F and Tn7_R primers indicated in
447 Table S4. The PCR was performed using Expand Long-Template Polymerase
448 (Roche) as described in the Supplementary Materials and Methods. Library
449 sequencing pools were sequenced on NextSeq and MiniSeq High Output SE75 runs
450 at the Petit Institute Molecular Evolution Core Facility at Georgia Institute of
451 Technology. Between 43,789 and 4,938,784 reads were obtained per sample.
452 Analysis script is available on github
453 (https://github.com/glew8/Barcode_Sequencing). Briefly, FastQC 0.11.7 and MultiQC
454 v1.5 were used to confirm sufficient sequencing quality [52,53]. Cutadapt 1.13 was used
455 to select only those sequences with the insert sequence, isolate barcode sequence,
456 and parse reads containing each barcode [54]. Then egrep was used to count reads
457 with each barcode. As a final check, FastQC was used to identify overrepresented
458 sequences that don't match any of the queried barcodes.
459
460 To identify the ancestor strain that the isolated RSCVs evolved from, colony PCRs
461 were performed using primers specific to each ancestor strain. The forward primer
462 contained the unique barcode used to tag each ancestor strain at the Tn7 site.

463 Therefore, for each RSCV, 6 PCRs were performed. Primers are indicated in Table
464 S4.
465
466 To identify mutations, genomic DNA was isolated from colony variants using the
467 DNeasy Blood and Tissue Kit (Qiagen) according to the manufactures protocol.
468 Clonal DNA was sequenced on an Illumina NextSeq 500 using a modified protocol
469 for library prep using the Illumina Nextera kit [55]. 2x151bp sequencing reads for
470 selected isolates were trimmed and quality filtered using Trimmomatic v0.36
471 (settings: LEADING:20 TRAILING:20 SLIDINGWINDOW:4:20 MINLEN:70) [56]. The
472 reads passing quality filtering were then used for variant calling with the open-source
473 program *breseq* v0.30.0 using default settings [57]. The reference sequences for
474 variant calling were acquired from NCBI's RefSeq database (NC_002516.2 for
475 PAO1, NC_008463.1 for PA14).
476
477 **Homology modelling**
478 The PA14 WspA sequence was obtained from the Pseudomonas genome database
479 [58]. The sequence was submitted to SWISS-MODEL using a template search [59].
480 Quality of the returned homology models was assessed on the Global Model Quality
481 Estimation (GMQE) score (numbers closer to 1 indicate more accurate model) and
482 the QMEAN score (numbers closer to 0 indicate that the model is comparable to
483 experimental structures). The homology model of PA14 WspA against the MCP of
484 *Thermotoga maritima* (PDB 3JA6; [32]) was determined to be the most accurate. The
485 homology model had a GMQE score of 0.37 and QMEAN score of -1.68.
486
487 **Prophage isolation and plaque assay**
488 To isolate prophages from B23-2, an overnight culture of B23-2 was diluted 1:100
489 and incubated for 30min at 37°C shaking at 200rpm. 0.5µg/mL of mitomycin C was
490 added to the culture and the OD_{600nm} was measured. The culture was re-incubated

and the OD_{600nm} measured every h. When the OD_{600nm} began to decrease the cells were pelleted by centrifugation and the supernatant filter sterilized and stored at 4°C.

To determine the level of susceptibility of *P. aeruginosa* strains to the bacteriophage(s) isolated from B23-2, 100 – 200µL of mid-log *P. aeruginosa* culture was incubated with 100µL serial dilutions of bacteriophage lysate for 15min at 37°C. The infection was added to 5mL molten soft agar (LB solidified with 0.7% agar) supplemented with 10mM $CaCl_2$ and $MgSO_4$. This was then poured over solidified hard agar (LB solidified with 1.5% agar), allowed to solidify and incubated overnight. The number of resulting plaques was then counted and PFU/mL determined.

Statistical Analysis

Data are presented as mean ± SD. To determine if data conformed to a normal distribution a Shapiro-Wilk test was performed. All of the data sets were normally distributed except for the PFU/mL data (Figure 5). For these data sets, means were compared using the non-parametric t-test. All other comparisons were made using a one-way ANOVA with a Tukey's post-hoc test and Student's t-test. Analyses were performed using GraphPad Prism v.5 (Graphpad Software). Statistical significance was determined using a p-value <0.05.

Data Availability

All sequencing reads from isolates are deposited in NCBI SRA under Bioproject number PRJNA491911 and Biosample accession numbers SAMN10101410 - SAMN10101459.

Acknowledgements. We would like to thank Michael Kann for his help with the planktonic and biofilm fitness assays.

519 **References**

520 1 Costerton, J. W. *et al.* Bacterial biofilms in nature and disease. *Annu Rev*
521 *Microbiol* **41**, 435-464, doi:10.1146/annurev.mi.41.100187.002251 (1987).
522 2 Hall-Stoodley, L., Costerton, J. W. & Stoodley, P. Bacterial biofilms: from the
523 natural environment to infectious diseases. *Nature reviews. Microbiology* **2**,
524 95-108, doi:10.1038/nrmicro821 (2004).
525 3 Hogardt, M. & Heesemann, J. Adaptation of Pseudomonas aeruginosa during
526 persistence in the cystic fibrosis lung. *International journal of medical*
527 *microbiology : IJMM* **300**, 557-562, doi:10.1016/j.ijmm.2010.08.008 (2010).
528 4 Lam, J., Chan, R., Lam, K. & Costerton, J. W. Production of mucoid
529 microcolonies by Pseudomonas aeruginosa within infected lungs in cystic
530 fibrosis. *Infection and immunity* **28**, 546-556 (1980).
531 5 Singh, P. K. *et al.* Quorum-sensing signals indicate that cystic fibrosis lungs
532 are infected with bacterial biofilms. *Nature* **407**, 762-764,
533 doi:10.1038/35037627 (2000).
534 6 Ciofu, O., Tolker-Nielsen, T., Jensen, P. O., Wang, H. & Hoiby, N.
535 Antimicrobial resistance, respiratory tract infections and role of biofilms in lung
536 infections in cystic fibrosis patients. *Advanced drug delivery reviews* **85**, 7-23,
537 doi:10.1016/j.addr.2014.11.017 (2015).
538 7 Evans, T. J. Small colony variants of Pseudomonas aeruginosa in chronic
539 bacterial infection of the lung in cystic fibrosis. *Future microbiology* **10**, 231-
540 239, doi:10.2217/fmb.14.107 (2015).
541 8 Haussler, S., Tummler, B., Weissbrodt, H., Rohde, M. & Steinmetz, I. Small-
542 colony variants of Pseudomonas aeruginosa in cystic fibrosis. *Clinical*
543 *infectious diseases : an official publication of the Infectious Diseases Society*
544 *of America* **29**, 621-625 (1999).
545 9 Thomassen, M. J., Demko, C. A., Boxerbaum, B., Stern, R. C. & Kuchenbrod,
546 P. J. Multiple isolates of Pseudomonas aeruginosa with differing antimicrobial
547 susceptibility patterns from patients with cystic fibrosis. *Journal of Infectious*
548 *Diseases* **140**, 873-880 (1979).
549 10 Drenkard, E. & Ausubel, F. M. Pseudomonas biofilm formation and antibiotic
550 resistance are linked to phenotypic variation. *Nature* **416**, 740-743 (2002).
551 11 Hengge, R. Principles of c-di-GMP signalling in bacteria. *Nature reviews.*
552 *Microbiology* **7**, 263-273, doi:10.1038/nrmicro2109 (2009).
553 12 Starkey, M. *et al.* Pseudomonas aeruginosa rugose small-colony variants
554 have adaptations that likely promote persistence in the cystic fibrosis lung.
555 *Journal of bacteriology* **191**, 3492-3503, doi:10.1128/jb.00119-09 (2009).
556 13 Kirisits, M. J., Prost, L., Starkey, M. & Parsek, M. R. Characterization of
557 colony morphology variants isolated from Pseudomonas aeruginosa biofilms.
558 *Applied and environmental microbiology* **71**, 4809-4821,
559 doi:10.1128/aem.71.8.4809-4821.2005 (2005).
560 14 Ma, L., Jackson, K. D., Landry, R. M., Parsek, M. R. & Wozniak, D. J.
561 Analysis of Pseudomonas aeruginosa conditional psl variants reveals roles
562 for the psl polysaccharide in adhesion and maintaining biofilm structure
563 postattachment. *Journal of bacteriology* **188**, 8213-8221,
564 doi:10.1128/jb.01202-06 (2006).
565 15 Mishra, M. *et al.* Pseudomonas aeruginosa Psl polysaccharide reduces
566 neutrophil phagocytosis and the oxidative response by limiting complement-
567 mediated opsonization. *Cellular microbiology* **14**, 95-106, doi:10.1111/j.1462-
568 5822.2011.01704.x (2012).
569 16 Pestrak, M. J. *et al.* Pseudomonas aeruginosa rugose small-colony variants
570 evade host clearance, are hyper-inflammatory, and persist in multiple host
571 environments. *PLoS pathogens* **14**, e1006842,
572 doi:10.1371/journal.ppat.1006842 (2018).

17 Boles, B. R., Thoendel, M. & Singh, P. K. Self-generated diversity produces "insurance effects" in biofilm communities. *Proc Natl Acad Sci U S A* **101**, 16630-16635, doi:10.1073/pnas.0407460101 (2004).

18 Flynn, K. M. *et al.* The evolution of ecological diversity in biofilms of Pseudomonas aeruginosa by altered cyclic diguanylate signaling. *Journal of bacteriology*, doi:10.1128/jb.00048-16 (2016).

19 Smith, E. E. *et al.* Genetic adaptation by Pseudomonas aeruginosa to the airways of cystic fibrosis patients. *Proceedings of the National Academy of Sciences* **103**, 8487-8492 (2006).

20 Huangyutitham, V., Guvener, Z. T. & Harwood, C. S. Subcellular clustering of the phosphorylated WspR response regulator protein stimulates its diguanylate cyclase activity. *mBio* **4**, e00242-00213, doi:10.1128/mBio.00242-13 (2013).

21 O'Connor, J. R., Kuwada, N. J., Huangyutitham, V., Wiggins, P. A. & Harwood, C. S. Surface sensing and lateral subcellular localization of WspA, the receptor in a chemosensory-like system leading to c-di-GMP production. *Molecular microbiology* **86**, 720-729, doi:10.1111/mmi.12013 (2012).

22 Guvener, Z. T. & Harwood, C. S. Subcellular location characteristics of the Pseudomonas aeruginosa GGDEF protein, WspR, indicate that it produces cyclic-di-GMP in response to growth on surfaces. *Molecular microbiology* **66**, 1459-1473, doi:10.1111/j.1365-2958.2007.06008.x (2007).

23 D'Argenio, D. A., Calfee, M. W., Rainey, P. B. & Pesci, E. C. Autolysis and autoaggregation in Pseudomonas aeruginosa colony morphology mutants. *Journal of bacteriology* **184**, 6481-6489 (2002).

24 Hickman, J. W., Tifrea, D. F. & Harwood, C. S. A chemosensory system that regulates biofilm formation through modulation of cyclic diguanylate levels. *Proc Natl Acad Sci U S A* **102**, 14422-14427, doi:10.1073/pnas.0507170102 (2005).

25 Roy, S. *et al.* Mixed-species biofilm compromises wound healing by disrupting epidermal barrier function. *The Journal of pathology* **233**, 331-343, doi:10.1002/path.4360 (2014).

26 Chaney, S. B. *et al.* Histopathological comparisons of Staphylococcus aureus and Pseudomonas aeruginosa experimental infected porcine burn wounds. *Wound repair and regeneration : official publication of the Wound Healing Society [and] the European Tissue Repair Society* **25**, 541-549, doi:10.1111/wrr.12527 (2017).

27 Friedman, L. & Kolter, R. Two genetic loci produce distinct carbohydrate-rich structural components of the Pseudomonas aeruginosa biofilm matrix. *Journal of bacteriology* **186**, 4457-4465 (2004).

28 Loytynoja, A. & Goldman, N. Short template switch events explain mutation clusters in the human genome. *Genome research* **27**, 1039-1049, doi:10.1101/gr.214973.116 (2017).

29 Rybtke, M. T. *et al.* Fluorescence-based reporter for gauging cyclic di-GMP levels in Pseudomonas aeruginosa. *Applied and environmental microbiology* **78**, 5060-5069, doi:10.1128/aem.00414-12 (2012).

30 Alexander, R. P. & Zhulin, I. B. Evolutionary genomics reveals conserved structural determinants of signaling and adaptation in microbial chemoreceptors. *Proceedings of the National Academy of Sciences* **104**, 2885-2890 (2007).

31 Ortega, D. R. *et al.* Assigning chemoreceptors to chemosensory pathways in Pseudomonas aeruginosa. *Proceedings of the National Academy of Sciences*, 201708842 (2017).

32 Cassidy, C. K. *et al.* CryoEM and computer simulations reveal a novel kinase conformational switch in bacterial chemotaxis signaling. *eLife* **4**, e08419 (2015).

33 Kelley, L. A., Mezulis, S., Yates, C. M., Wass, M. N. & Sternberg, M. J. The Phyre2 web portal for protein modeling, prediction and analysis. *Nature protocols* **10**, 845 (2015).

34 Cady, K. *et al.* Prevalence, conservation and functional analysis of Yersinia and Escherichia CRISPR regions in clinical Pseudomonas aeruginosa isolates. *Microbiology (Reading, England)* **157**, 430-437 (2011).

35 Barrangou, R. & Marraffini, L. A. CRISPR-Cas systems: prokaryotes upgrade to adaptive immunity. *Molecular cell* **54**, 234-244 (2014).

36 Khan, A. I., Dinh, D. M., Schneider, D., Lenski, R. E. & Cooper, T. F. Negative epistasis between beneficial mutations in an evolving bacterial population. *Science (New York, N.Y.)* **332**, 1193-1196 (2011).

37 Cooper, V. S., Staples, R. K., Traverse, C. C. & Ellis, C. N. Parallel evolution of small colony variants in Burkholderia cenocepacia biofilms. *Genomics* **104**, 447-452, doi:10.1016/j.ygeno.2014.09.007 (2014).

38 Rainey, P. B. & Rainey, K. Evolution of cooperation and conflict in experimental bacterial populations. *Nature* **425**, 72 (2003).

39 Rainey, P. B. & Travisano, M. Adaptive radiation in a heterogeneous environment. *Nature* **394**, 69 (1998).

40 Kim, W., Levy, S. B. & Foster, K. R. Rapid radiation in bacteria leads to a division of labour. *Nature communications* **7**, 10508 (2016).

41 Hogardt, M. & Heesemann, J. Adaptation of Pseudomonas aeruginosa during persistence in the cystic fibrosis lung. *International Journal of Medical Microbiology* **300**, 557-562 (2010).

42 Cady, K. C., Bondy-Denomy, J., Heussler, G. E., Davidson, A. R. & O'Toole, G. A. The CRISPR/Cas adaptive immune system of Pseudomonas aeruginosa mediates resistance to naturally occurring and engineered phages. *Journal of bacteriology*, JB. 01184-01112 (2012).

43 Ueda, A. & Wood, T. K. Connecting quorum sensing, c-di-GMP, pel polysaccharide, and biofilm formation in *Pseudomonas aeruginosa* through tyrosine phosphatase TpbA (PA3885). *PLoS Path.* **5**, e1000483 (2009).

44 Malone, J. G. *et al.* YfiBNR mediates cyclic-di-GMP dependent small colony variant formation and persistence in *Pseudomonas aeruginosa*. *PLoS Path.* **6**, e1000804 (2010).

45 Giddens, S. R. *et al.* Mutational activation of niche-specific genes provides insight into regulatory networks and bacterial function in a complex environment. *Proc. Natl. Acad. Sci. U. S. A.* **104**, 18247-18252 (2007).

46 Jones, C. J. *et al.* ChIP-Seq and RNA-Seq reveal an AmrZ-mediated mechanism for cyclic di-GMP synthesis and biofilm development by *Pseudomonas aeruginosa*. *PLoS Path.* **10**, e1003984, doi:10.1371/journal.ppat.1003984 (2014).

47 Irie, Y. *et al. Pseudomonas aeruginosa* biofilm matrix polysaccharide Psl is regulated transcriptionally by RpoS and post-transcriptionally by RsmA. *Mol. Microbiol.* **78**, 158-172 (2010).

48 Gibson, D. G. *et al.* Enzymatic assembly of DNA molecules up to several hundred kilobases. *Nature methods* **6**, 343-345 (2009).

49 Choi, K.-H. & Schweizer, H. P. An improved method for rapid generation of unmarked Pseudomonas aeruginosa deletion mutants. *BMC microbiology* **5**, 30 (2005).

50 Cooper, V. S. Experimental Evolution as a High-Throughput Screen for Genetic Adaptations. *mSphere* **3**, doi:10.1128/mSphere.00121-18 (2018).

51 Schindelin, J. *et al.* Fiji: an open-source platform for biological-image analysis. *Nature methods* **9**, 676 (2012).

52 Andrews, S. FastQC: a quality control tool for high throughput sequence data. (2010).

53 Ewels, P., Magnusson, M., Lundin, S. & Käller, M. MultiQC: summarize analysis results for multiple tools and samples in a single report. *Bioinformatics* **32**, 3047-3048 (2016).

54 Martin, M. Cutadapt removes adapter sequences from high-throughput sequencing reads. *EMBnet. journal* **17**, pp. 10-12 (2011).

55 Baym, M. *et al.* Inexpensive multiplexed library preparation for megabase-sized genomes. *PloS one* **10**, e0128036, doi:10.1371/journal.pone.0128036 (2015).

56 Bolger, A. M., Lohse, M. & Usadel, B. Trimmomatic: a flexible trimmer for Illumina sequence data. *Bioinformatics* **30**, 2114-2120 (2014).

57 Deatherage, D. E. & Barrick, J. E. in *Engineering and analyzing multicellular systems* 165-188 (Springer, 2014).

58 Winsor, G. L. *et al.* Enhanced annotations and features for comparing thousands of Pseudomonas genomes in the Pseudomonas genome database. *Nucleic acids research* **44**, D646-D653 (2015).

59 Guex, N., Peitsch, M. C. & Schwede, T. Automated comparative protein structure modeling with SWISS‐MODEL and Swiss‐PdbViewer: A historical perspective. *Electrophoresis* **30** (2009).

719 **Table 1: Mutations identified in PA14-1 RSCVs**

Sample			Driver mutation			Secondary mutation	
Day	**RSCV #**	**Wound#**	**Gene**	**Mutation[a]**	**Freq (%)**	**Gene**	**Mutation**
3	1	1	*wspA*	285-298del		*pslO-pslE*	Δ14,299 bp
	2	2	*wspA*	285-298del			
						pslO-pslE	Δ14,299 bp
	4	1	*wspA*	285-298del		PA14_13130/PA14_13140	TNN→TGC
						fabI/ppiD	TTC → TCC
Day 3 summary			*wspA*	285-298del	100		
14	3	4	*wspA*	285-298del			
	6	4	*wspA*	285-298del			
	7	4	*wspA*	285-298del			
	8	4	*wspA*	285-298del			
	9	4	*wspA*	285-298del			
	10	4	*wspA*	285-298del			
	12	4	*wspA*	285-298del		CRISPR-Cas1/hp	+60bp
						glutamyl-tRNA reductase	L71L (CTG→TTG)
	13	1	*wspA*	285-298del		*fabI/ppiD*	TTC → TCC
	14	4	*wspA*	285-298del			
	16	4	*wspA*	285-298del			
	17	4	*wspA*	285-298del			
	20	4	*wspF*	V154fs			
	24	1	*wspA*	285-298del			
	27	1	*wspA*	285-298del			
	28	2	*wspA*	285-298del			
	36	3	*wspF*	V154fs			
	37	3	*wspA*	285-298del			
	38	3	*wspF*	V154fs		CRISPR-Cas1/hp	+60bp
	86	3	*wspA*	285-298del			
Day 14 summary			*wspA*	285-298del	84.2		
			wspF	V154fs	15.8		
28	40	1	*wspA*	285-298del		*wspD*	1 bp→TT
							2 bp→AG
							S197S (TCG→TCA)
						PA14_54090	A248V (GCG→GTG)
	42	3	*wspA*	285-298del			
	43	3	*wspA*	285-298del			
	45	3	*wspA*	285-298del			
	87	2	*wspA*	285-298del			
Day 28 summary			*wspA*	285-298del	100		

720 [a] Deleted amino acid residues are indicated

721 del: deletion, fs: frame shift, hp: hypothetical protein

722

723 **Figure legends**

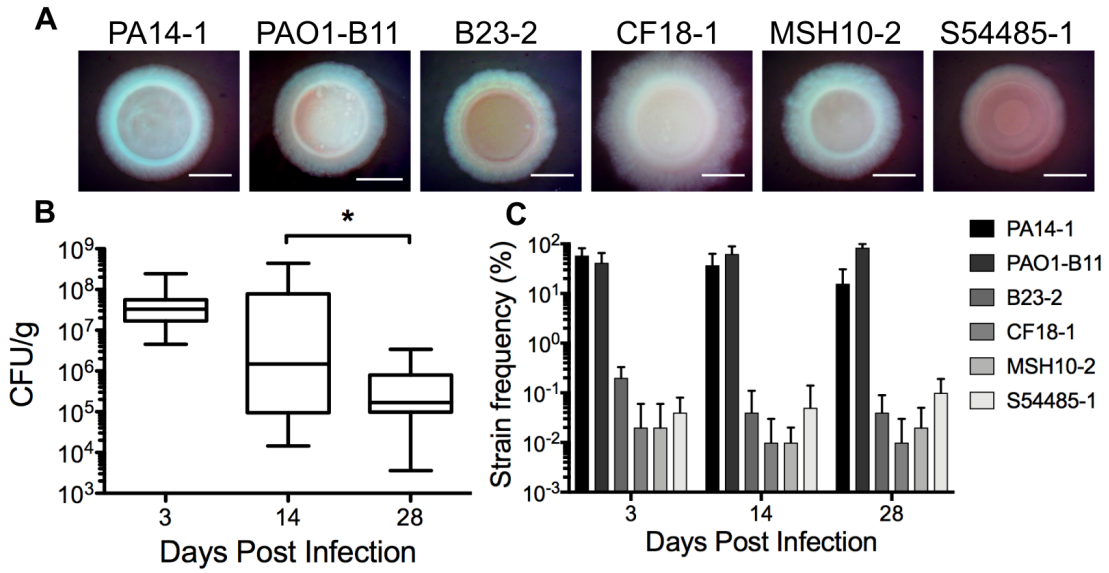

724

725 **Figure 1: *P. aeruginosa* burden in a mixed-strain chronic burn wound infection**

726 **(A)** Colony morphology on VBMM of the 6 *P. aeruginosa* strains used to infect
727 porcine burn wounds. Scale bar 2mm. **(B)** Biopsies were taken from wounds at 3, 14
728 and 28-d. Biopsies were homogenized and plated for CFU/g. Each biopsy was plated
729 in triplicate, with a minimum of 4 biopsies taken from each wound. * p-value <0.05.
730 **(C)** Genomic DNA was isolated from homogenized biopsies and the strain specific
731 barcodes at the *Tn7* site sequenced. The proportion of strain barcodes was
732 expressed as a percentage of the total sequence reads to determine the relative
733 frequency of each strain during the infection. A minimum of 4 biopsies from each
734 wound was sequenced.

735

736

737

738

739

740

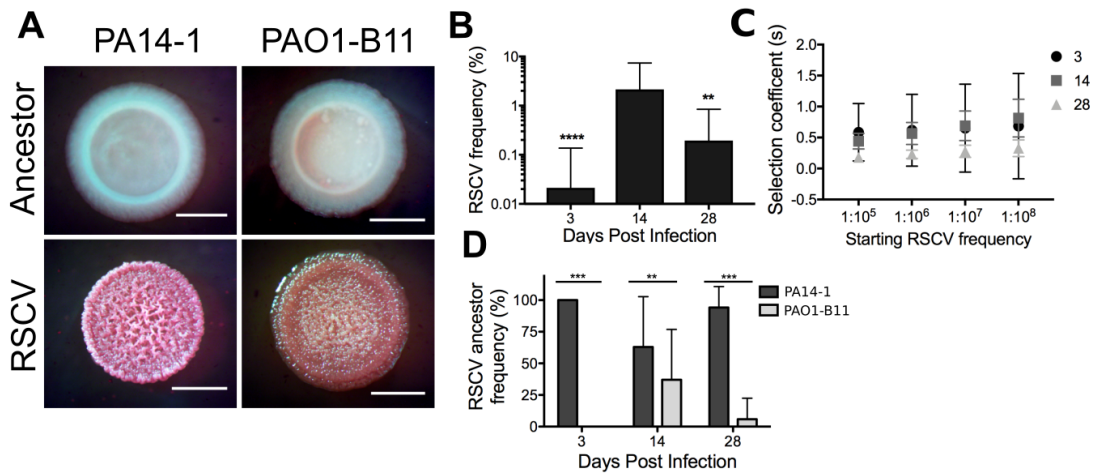

741

742 **Figure 2: *P. aeruginosa* RSCVs isolated from porcine chronic burn wound**
743 **infections. (A)** Representative colony morphologies of RSCVs isolated from
744 homogenized porcine burn wound tissue. RSCVs were plated on VBMM and the
745 colony morphology was compared to the ancestor strain (labelled). Scale bar 2mm.
746 **(B)** Frequencies of RSCVs isolated at each timepoint, expressed as a percentage of
747 the total *P. aeruginosa* population. Data presented as mean ± SD. ** p-value <0.01,
748 **** p-value <0.0001 compared to 14-d. **(C)** Selection coefficient (*s*) of RSCVs in the
749 wound determined at each timepoint across a range of starting frequencies at t=0.
750 **(D)** Frequency of the ancestor strain that the RSCVs evolved from, expressed as a
751 percentage of the total RSCV sub-population. Data presented as mean ± SD. ** p-
752 value <0.01, *** p-value <0.001.

753

754

755

756

757

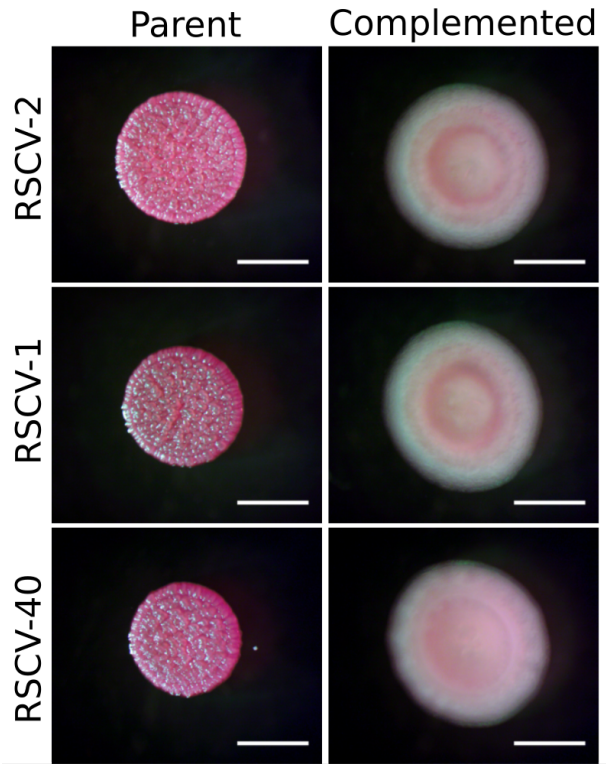

Figure 3: Complementation of the *wspA*Δ42bp mutation. *wspA* was complemented in representative RSCVs by replacing *wspA* Δ285-298 with a wildtype copy on the genome. RSCV-2 was selected as a representative RSCV with the *wspA* driver mutation alone. RSCV-1 and RSCV-40 have the *wspA* driver mutation as well as Δ*pslE-pslO* and *wspD* secondary mutations, respectively. Parent and complemented RSCVs (labeled) were grown on VBMM and colony morphology was assessed. Scale bar 2mm.

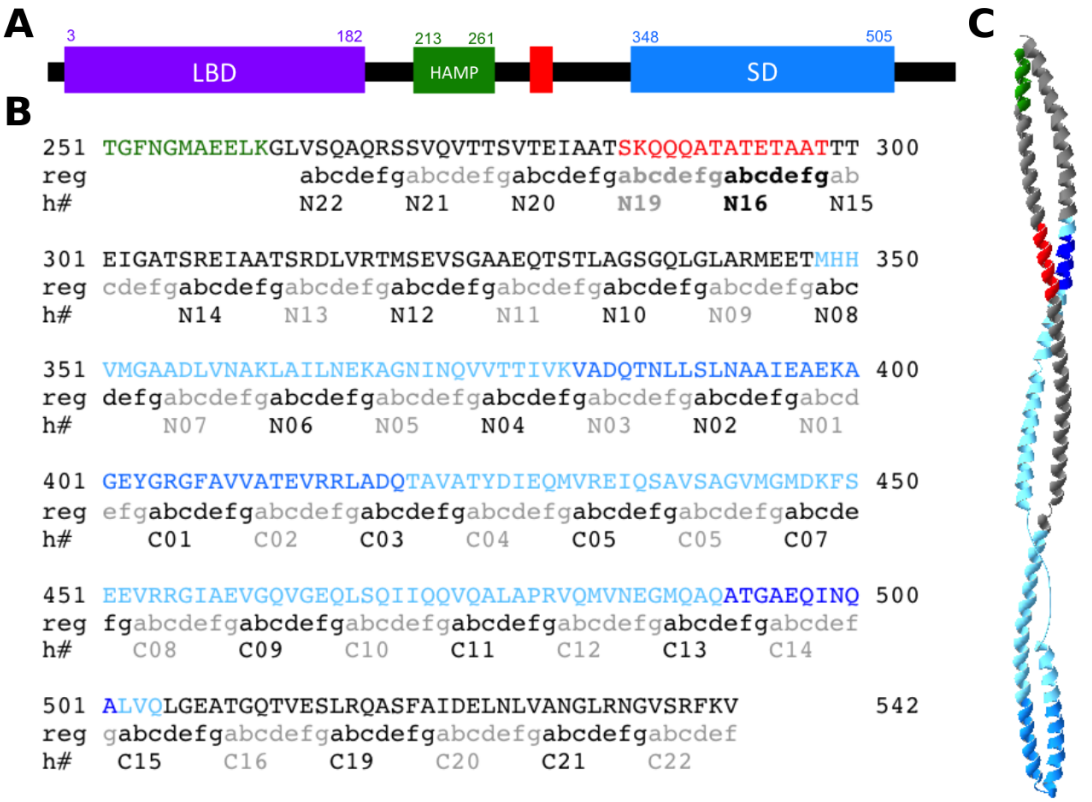

Figure 4: 14aa deletion in WspA is predicted to occur opposite the methylation site. (A) Schematic of WspA. The different domains of WspA were determined from the Pseudomonas Genome Database [58] Pfam analysis. LBD = ligand binding domain or the four helix bundle domain (3-182aa). HAMP = linker domain (213-261aa). SD = MCP signaling domain (348-505aa). The region of the 14aa deletion is indicated in red (285-298aa). **(B)** The WspA cytoplasmic domain amino acid sequence. The full amino acid sequence and predicted secondary structure of WspA is depicted in Fig S6. The domains are indicated by the same colors in **(A)**. The signaling domain contains two additional features, the kinase interacting subdomain, or 'tip' domain in dark blue (382-420aa) and the predicated methylation site in navy blue (492-501aa) [31]. Both the heptad registers (reg) and the heptad number (h#) are labeled [30,31], with consecutive hetpads indicated in alternating black and grey text. **(C)** Homology model of PA14 WspA modeled against the *T. maritime* MCP (PDB 3JA6; [32])

generated using SWISS-MODEL [59]. Colors correspond to the domains indicated in **(B)**. Model spans 250-541aa of WspA.

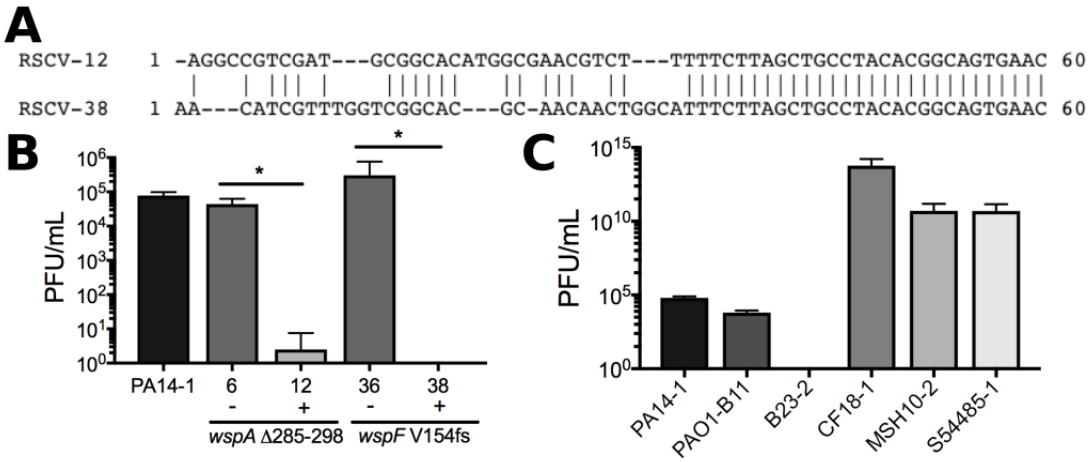

Figure 5: RSCV-12 and RSCV-38 are resistant to infection by phage isolated from B23-2. (A) The 60bp insertion sequence in the CRISPR array of RSCV-12 and RSCV-38. Prophages were isolated from B23-2 and plaque assays were performed to determine the level of phage infection for **(B)** representative RSCV isolates and **(C)** the ancestor wildtype *P. aeruginosa* strains. RSCV-6 and RSCV-12 both have the same driver *wspA* mutation, while RSCV-36 and RSCV-38 have the same driver *wspF* mutation. ± indicates the presence/absence of the CRISPR insertion. The driver mutation for each RSCV is labelled. Data presented as mean ± SD, n=4. * p-value <0.05.